IEEE Access
Multidisciplinary | Rapid Review | Open Access Journal

Received February 12, 2022, accepted February 26, 2022, date of publication February 28, 2022, date of current version March 8, 2022.

Digital Object Identifier 10.1109/ACCESS.2022.3155694

Initial-Rectification Barrier Iterative Learning Control for Pneumatic Artificial Muscle Systems With Nonzero Initial Errors and Iteration-Varying Reference Trajectories

YOUFANG YU AND SONGHONG LAI
Applied Engineering College, Zhejiang Business College, Hangzhou 310053, China
Corresponding author: Youfang Yu (youfang_yu@163.com)

This work was supported in part by the Key Research and Development Project of Zhejiang Province under Grant 2019C02080, in part by the Project from the Education Department of Zhejiang Province under Grant Y202044860, and in part by the Visiting Scholar Project from the Education Department of Zhejiang Province under Grant FX2019077.

ABSTRACT Pneumatic artificial muscle actuators possess great potential in compliant rehabilitation devices since they are flexible and lightweight. The inherent high nonlinearities, uncertainties, hysteresis and time-varying characteristics in pneumatic artificial muscle systems brings much challenge for accurate system modeling and controller design. The angle tracking problem based on iterative learning control technology is considered in this work. This research proposes a new initial-rectification adaptive iterative learning control scheme for a pneumatic artificial muscle-actuated device with nonzero initial errors and iteration-varying reference trajectories. A barrier Lyapunov function is used to deal with the constraint requirement. A new initial rectification construction method is given to solve the nonzero initial error problem. Nonparametric uncertainties in the system are approximated by using a neural network, whose optimal weight is estimated by using difference learning method. As the iteration number increases, the system states of angle and angular velocity can accurately track the reference trajectories over the whole interval, respectively. In the end, the simulation results show excellent trajectory tracking performance of the iterative learning controller even if the reference trajectories are non-repetitive over the iteration domain.

INDEX TERMS Pneumatic artificial muscle systems, iterative learning control, initial rectification approach, barrier Lyapunov function.

I. INTRODUCTION

As a kind of tube-like actuators, pneumatic artificial muscle(PAM) actuators can contract or extend like real human muscles by inflating and deflating pressurized air through servo valves. The innate compliance and muscle elasticity of PAM actuators provide safe and soft interactions. The characteristic of low weight and flexibility of PAM actuators make them suitable for reconfigurable, compact and portable applications [1], [2]. Traditional electric and hydraulic actuators exhibit high stiffness, but are too heavy and rigid for medical rehabilitation and wearable applications. Due to the inherent features of high nonlinearities, complex hysteresis, and time-varying characteristics, achieving high-precision trajectory tracking control performance for PAM systems is not easy such that PAM actuators have not been extensively used in robotics to date even if they possess the obvious advantages over conventional actuators. To obtain satisfactory control performance, attempts have been made in the past two decades [3]–[12]. Up to now, the high-precision control of PAM systems is still a challenging issue.

Iterative learning control (ILC) technology has been put forward in the early 1980s. According to the system errors in the previous iteration(s), the control precisions of ILC systems may be gradually improved by updating the leaning parameters or control inputs, cycle by cycle, and better control performances may be obtained even without using accurate system models [13]–[22]. The special working

The associate editor coordinating the review of this manuscript and approving it for publication was Mou Chen.

principle of ILC bring continuous attention during the past serval decades. So far, ILC has been regarded as one of the most effective control strategies in handling repeated tracking control tasks or rejecting periodic disturbances for nonlinear systems, and has been applied in numerous practical applications, such as servo motors, robot manipulators, batch chemical process and traffic flows [23]–[25]. In the field of ILC, adaptive ILC, which can be seen as a combination of ILC and adaptive control, has been a hot topic since this century.

We will consider three important aspects in the research of ILC on PAM systems. The initial position problem of PAM ILC systems is the first issue that we will discuss. Theoretically speaking, for an ILC system, through continuous iterations by using the error information in the previous iteration(s), the control performance may get better and better during the whole operation time interval. However, in most traditional ILC algorithms, the above-mentioned excellent control performance is based on the premise that the initial error of ILC systems in each iteration should be zero; if the premise can not be satisfied, system divergence may occur even if the initial error is very slight. For the limitations of physical resetting, the zero initial error cannot be realized in practical applications. Consequently, how to design ILC controllers under nonzero initial error conditions, is a fundamental research issue in the field of ILC, which is usually be called initial position problem of ILC. In the context of PAM systems, the research on the initial position problem is still preliminary at present. Guo *et al.* proposed a robust adaptive ILC scheme to solve the angle tracking problem for a kind of PAM-actuated mechanism, with alignment condition used to solve the initial position problem [26]. Yang *et al.* design an angle error-track adaptive ILC algorithm solve the angle tracking problem for a PAM system with nonzero initial errors [27]. Overall, the number corresponding results is very limited. The initial position problem of PAM ILC systems is an issue worthy to be further studied.

The repetitiveness of reference trajectories for PAM ILC systems is another concern that we want to address. In most traditional ILC algorithms, a controlled system is assumed to perform a same specific control task during all iterations, i.e., the reference trajectory for a control system must be iteration-invariant. However, in practical applications, there exists the requirements on tracking iteration-varying reference trajectories to improve the efficiencies or match the technical processes. The earlier studies on iteration-varying trajectory tracking were reported in [28] on contraction-mapping ILC with slow iteration-varying reference trajectories, and in [29] on adaptive ILC with iteration-varying reference trajectories, respectively. On the basis of above works, some scholars continued in-depth research on adaptive ILC with iteration-varying reference trajectories [30]- [35]. In the context of PAM systems, the research on this issue is still a research blank at present.

In addition, the constraint requirement in ILC systems is also an interesting issue. For the purpose of system specifications and safety considerations, the system output, the system state, or the output tracking error should be constrained in some situations. Inspired by the development in barrier Lyapunov function-based adaptive control [36], [37], Jin and Xu carried out the earlier investigation on state-constrained adaptive ILC [38] and output-constrained ILC [39]. Later on, some further results on barrier ILC have been reported, such as barrier error-tracking state-constrained ILC [40], state and input-constraint ILC [41], constrained data-driven optimal iterative learning control [42], joint position constrained robotic ILC [43], constrained spatial adaptive ILC [44], [45]. None of these works consider the state/output constraint ILC for PAM systems. How to develop an effective ILC algorithm to deal with PAM system under nonzero initial errors, as well as to meet the requirement of iteration-varying trajectory tracking and system constraint during operation, has not been addressed yet.

In this work, we present a novel barrier adaptive ILC scheme for a PAM system with nonzero initial errors, iteration-varying reference trajectories and constraint requirements on angle/angle velocity tracking error. The main results and contributions of this work can be summarized as follows.

(1) A news construction method of rectification reference trajectories is presented to deal with initial position problem of PAM ILC system.

(2) The constraint requirement on angle/angluar velocity is implemented by using barrier Lyapunov function approach during the ILC design for the PAM system.

(3) By constructing a novel Lyapunov−Krasovskii functional, an adaptive ILC law is developed to address the iteration-varying trajectory tracking for the PAM ILC system.

The rest of this paper is organized as follows. The problem formulation is introduced in Section II. The detailed procedure of controller design is addressed in Section III. The convergence analysis of closed-loop PAM systems is given in Section IV. In Section V, the simulation results are illustrated to verify the effectiveness of the proposed control scheme. Finally, Section VI concludes this work.

II. PROBLEM FORMULATION

Consider the angle tracking problem of a PAM-actuated device as shown in Fig. 1. The main component of this device includes an air compressor, two proportional valves, two PAM actuators, an angle sensor and a computer. In this PAM system, the control commands which are dictated from the computer can be sent to the two proportional valves. The computer queries the deflection angle of pulley through the sensor in real time. By opening and closing of the two valves, the force may be generated by the pressurized air inside PAM actuators.

The two control variables of this system may be described as

$$\begin{cases} u_l(t) = u_o + c_u u(t), \\ u_r(t) = u_o - c_u u(t), \end{cases} \tag{1}$$

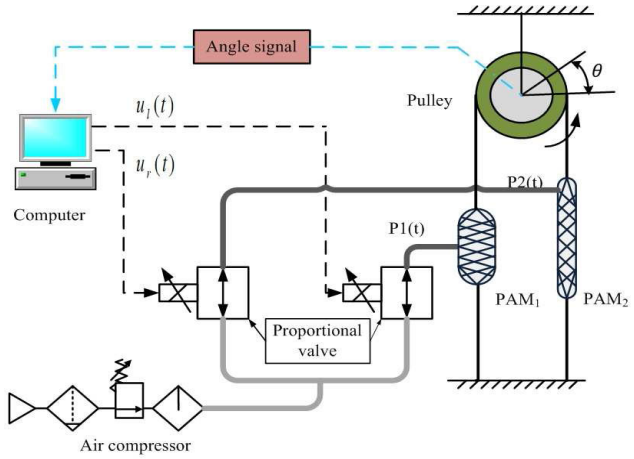

FIGURE 1. The control structure of PAM-actuated device.

in which $u_o(t)$ is the initial preloaded control voltage, c_u is the voltage distribution coefficient, and $u(t)$ is the control input. The internal air pressures of actuators are determined by the property as follows:

$$\begin{cases} P_1(t) = P_0 + \Delta P(t) = c_0 u_l(t), \\ P_2(t) = P_0 - \Delta P(t) = c_0 u_r(t), \end{cases} \tag{2}$$

where $P_1(t)$ and $P_2(t)$ are the internal pressures of two PAM actuators, respectively; P_0 is the preloaded internal pressure, and ΔP is the variation of pressure. The relationship between the pulling forces and the internal air pressures of actuators may be expressed as follows:

$$\begin{cases} F_1(t) = P_1(t)(c_1\epsilon_1^2(t) + c_2\epsilon_1(t) + c_3) + c_4, \\ F_2(t) = P_2(t)(c_1\epsilon_2^2(t) + c_2\epsilon_1(t) + c_3) + c_4, \end{cases} \tag{3}$$

where $F_1(t)$ and $F_2(t)$ are two pulling forces of PAM actuators, c_1-c_4 are four parameters, and $\epsilon_1(t)$ and $\epsilon_2(t)$ are derived according to (4).

$$\begin{cases} \epsilon_1(t) = \epsilon_0 + r l_0^{-1}\theta(t), \\ \epsilon_2(t) = \epsilon_0 - r l_0^{-1}\theta(t), \end{cases} \tag{4}$$

where $\theta(t)$ and r are the deflection angle and the radius of pulley, respectively; ϵ_0 and l_0 are the initial shrinking rate and initial length of PAM actuators, respectively. The driving moment $T_p(t)$ of the device may be deduced from the following equation as

$$\begin{aligned} T_p(t) &= J_p\ddot{\theta}(t) + b_p\dot{\theta}(t) \\ &= F_1(t)r - F_2(t)r + d_p(\theta(t), \dot{\theta}(t), t), \end{aligned} \tag{5}$$

where J_p is the moment of inertia, b_p is the damping coefficient, and $d_p(\theta(t), \dot{\theta}(t), t)$ denotes unmodeled dynamics. Substituting (1)-(4) into (5) yields

$$\begin{aligned} &J_p\ddot{\theta}(t) + b_p\dot{\theta}(t) \\ &= c_0 u_o r(4c_1\epsilon_0 r l_0^{-1} + 2c_2 r l_0^{-1})\theta(t) + c_0 c_u r\big[2c_1\epsilon_0^2 \\ &\quad + 2c_1(r\theta(t)l_0^{-1})^2 + 2c_2\epsilon_0 + 2c_3\big]u(t) + d_p(\theta(t), \dot{\theta}(t), t) \end{aligned} \tag{6}$$

In the following of this paper, $d_p(\theta(t), \dot{\theta}(t), t)$ is abbreviated as d_p, and function arguments are sometimes omitted when no confusion arises. In real situations, the defection angle $\theta(t)$ is very small, such that $2c_1(r\theta(t)l_0^{-1})^2 \approx 0$ [4] and then (6) can be rewritten as

$$\begin{aligned} \ddot{\theta}(t) = &-\frac{b_p}{J_p}\dot{\theta}(t) + \frac{2c_0 u_o r^2(2c_1\epsilon_0 + c_2)l_0^{-1}}{J_p}\theta(t) \\ &+ \frac{2c_0 c_u r(c_1\epsilon_0^2 + c_2\epsilon_0 + c_3)}{J_p}u(t) + \frac{d_p}{J_p}. \end{aligned} \tag{7}$$

Let $x_1(t) = \theta(t)$, $x_2(t) = \dot{\theta}(t)$ and $y(t) = x_1(t)$. From (7), we get the state-space model of PAM systems during the kth iteration as

$$\begin{cases} \dot{x}_{1,k} = x_{2,k}, \\ \dot{x}_{2,k} = u_{o,k}\eta_1 x_{1,k} + \eta_2 x_{2,k} + g u_k + \dfrac{d_{p,k}}{J_p} \\ y_k = x_{1,k} \end{cases} \tag{8}$$

where $\eta_1 = \frac{2k_0 r^2(2k_1\epsilon_0 + k_2)l_0^{-1}}{J_p}$, $\eta_2 = -\frac{b_p}{J_p}$ and $g = \frac{2k_0 k_u r(k_1\epsilon_0^2 + k_2\epsilon_0 + k_3)}{J_p}$.

Let $\boldsymbol{x}_k = [x_1, x_2]^T$, $\boldsymbol{x}_d = [x_{1d}, x_{2d}] = [y_d, \dot{y}_d]^T$ and $\boldsymbol{e}_k = [e_{1,k}, e_{2,k}]^T = \boldsymbol{x}_k - \boldsymbol{x}_d$. The control task of this work is to let y_k accurately track y_d over $[0, T]$ while $\boldsymbol{e}_k(0) = 0$ cannot be guaranteed, as the iteration index k increases.

III. CONTROLLER DESIGN

In order to achieve the control objective, our control strategy is to make $\boldsymbol{x}_k(t)$ follow the initial-rectification reference trajectory $\boldsymbol{x}_{rk}(t) = [x_{r1,k}(t), x_{r2,k}(t)]$ for $t \in [0, T]$, which is formed as follows:

$$x_{r1,k}(t) = x_{1,d}(t) + \omega(t)e_{1,k}(0) + \omega(t)te_{2,k}(0), \tag{9}$$

$$x_{r2,k}(t) = \dot{x}_{1,d}(t) + \dot{\omega}(t)e_{1,k}(0) + [\omega(t) + \dot{\omega}(t) \times t]e_{2,k}(0), \tag{10}$$

where

$$\omega(t) = \begin{cases} (1 - \dfrac{t}{t_\omega})^3, & \text{if } 0 \le t \le t_\omega, \\ 0, & \text{if } t_\omega < t \le T. \end{cases}$$

According to the construction in (9)-(10), x_{rk} possesses the following properties: i) $\boldsymbol{x}_{rk}(0) = \boldsymbol{x}_k(0)$; ii) $\boldsymbol{x}_{rk}(t) = \boldsymbol{x}_k(t)$ for $t \in [t_\omega, T]$; iii) $x_{r2,k}(t) = x_{r1,k}(t)$ and $\boldsymbol{x}_{rk}(t)$ is differentiable for $t \in (0, T)$.

Define $\boldsymbol{e}_{r,k} = [e_{r1,k}, e_{r2,k}]^T = \boldsymbol{x}_k - \boldsymbol{x}_{r,k}$. Note that $\boldsymbol{e}_{r,k}(0) = 0$ holds, which is of significance to carry out the controller design in the next step. From (8), we have

$$\begin{cases} \dot{e}_{r1,k} = e_{r2,k}, \\ \dot{e}_{r2,k} = u_{o,k}\eta_1 x_{1,k} + \eta_2 x_{2,k} + g u_k + \dfrac{d_{p,k}}{J_p} - \dot{x}_{r2,k}. \end{cases} \tag{11}$$

Let $s_{r,k} = \lambda e_{r1,k} + e_{r2,k}$ with $\lambda > 0$. Obviously, $s_{r,k}(0) = 0$.

Define a barrier Lyapunov function

$$V_k(t) = \frac{1}{2}\frac{s_{r,k}^2}{b_s^2 - s_{r,k}^2}, \tag{12}$$

with $b_s > 0$. Taking its time derivative with respect to t yields

$$\begin{aligned}\dot{V}_k &= \sigma_k s_{r,k} g\big[g^{-1}\lambda e_{r2,k} + g^{-1}u_{o,k}\eta_1 x_{1,k} + g^{-1}\eta_2 x_{2,k} + u_k \\ &\quad + \frac{d_{p,k}}{gJ_p} - g^{-1}\dot{x}_{r2,k}\big] \\ &= \sigma_k s_{r,k} g(\boldsymbol{\varpi}^T\boldsymbol{\xi}_k + u_k + \frac{d_{p,k}}{gJ_p}),\end{aligned} \tag{13}$$

in which $\sigma_k = \frac{b_s^2}{(b_s^2 - s_{\phi k}^2)^2}$, $\boldsymbol{\varpi} \triangleq [g^{-1}, g^{-1}\eta_1, g^{-1}\eta_2, g^{-1}]^T$ and $\boldsymbol{\xi}_k \triangleq [\lambda e_{r2,k}, u_{o,k}x_{1,k}, x_{2,k}, \dot{x}_{r2,k}]^T$.

Then, radial basis function (RBF) neural network is applied to approximate $\frac{d_{p,k}}{gJ_p}$ as follows:

$$\frac{d_{p,k}}{gJ_p} = \boldsymbol{w}^{*T}(t)\boldsymbol{\varphi}(\boldsymbol{X}_k) + \epsilon(\boldsymbol{X}_k), \tag{14}$$

where $\boldsymbol{w}^*(t)$ is the ideal weight of neural network, $\epsilon(\boldsymbol{X}_k)$ is the approximation error of neural network, $\boldsymbol{X}_k = [e_{r1,k}, e_{r2,k}, x_{r1,k}, x_{r2,k}, \dot{x}_{r2,k}]^T$, $|\epsilon(\boldsymbol{x}_k)| \le \epsilon_N$, and $\boldsymbol{\varphi}(\boldsymbol{x}_k) = [\varphi_{1,k}, \varphi_{2,k}, \cdots, \varphi_{m,k}]^T$ with

$$\varphi_{j,k} = \mathrm{e}^{-\frac{\|\boldsymbol{X}_k - \boldsymbol{c}_j\|^2}{2b_j^2}}, \quad j = 1, 2, \cdots, m. \tag{15}$$

Here, $\boldsymbol{c}_j$ and b_j are the center vector and the width of the hidden layer, respectively. Combining (13) with (14) yields

$$\begin{aligned}\dot{V}_k \le \sigma_k s_{r,k} g(\boldsymbol{\varpi}^T\boldsymbol{\xi}_k + u_k) + \sigma_k s_{r,k} g\boldsymbol{w}^{*T}(t)\boldsymbol{\varphi}(\boldsymbol{x}_k) \\ + \sigma_k s_{r,k} g\epsilon_N,\end{aligned} \tag{16}$$

Let $\boldsymbol{\varphi}_k$ be the abbreviation of $\boldsymbol{\varphi}(\boldsymbol{x}_k)$. On the basis of (16), we design control law and learning laws as follows:

$$\begin{aligned}u_k &= -\gamma_1 s_{r,k} - \boldsymbol{\varpi}_k^T\boldsymbol{\xi}_k - \boldsymbol{w}_k^T\boldsymbol{\varphi}_k - \epsilon_{N,k}\tanh(\sigma_k\epsilon_{N,k} \\ &\quad \times (k+1)^2 s_{r,k}) \qquad (17) \\ \boldsymbol{\varpi}_k &= \mathrm{sat}_{\underline{\varpi},\bar{\varpi}}(\boldsymbol{\varpi}_{k-1}) + \gamma_2\sigma_k s_{\phi,k}\boldsymbol{\xi}_k, \boldsymbol{\varpi_{-1}} = 0, \qquad (18) \\ \boldsymbol{w_k} &= \mathrm{sat}_{\underline{w},\bar{w}}(\boldsymbol{w}_{k-1}) + \gamma_3\sigma_k s_{\phi,k}\boldsymbol{\varphi}_k, \boldsymbol{w_{-1}} = 0, \qquad (19) \\ \epsilon_{N,k} &= \mathrm{sat}_{0,\bar{\epsilon}_N}(\epsilon_{N,k-1}) + \gamma_4\sigma_k|s_{r,k}|, \epsilon_{N,-1} = 0, \qquad (20)\end{aligned}$$

where $\gamma_1 > 0$, $\gamma_2 > 0$, $\gamma_3 > 0$, $\gamma_4 > 0$, and $\epsilon_{N,k}$ is used to estimate ϵ_N. For a scalar $\hat{\beta}$, which is the estimation to a scalar β,

$$\mathrm{sat}_{\underline{\beta},\bar{\beta}}(\hat{\beta}) := \begin{cases}\bar{\beta}, & \text{if } \hat{a} > \bar{\beta} \\ \hat{\beta}, & \text{if } \underline{\beta} \le \hat{\beta} \le \bar{\beta} \\ \underline{\beta}, & \text{if } \hat{\beta} < \underline{\beta}\end{cases},$$

where $\underline{\beta}$ and $\bar{\beta}$ are the lower bound and upper bound of the scalar β, respectively. For a vector $\hat{\boldsymbol{\beta}} = [\hat{\beta}_1, \hat{\beta}_2, \cdots, \hat{\beta}_m] \in \mathbb{R}^m$, $\mathrm{sat}_{\underline{\beta},\bar{\beta}}(\hat{\boldsymbol{\beta}}) := \big[\mathrm{sat}_{\underline{\beta},\bar{\beta}}(\hat{\beta}_1), \mathrm{sat}_{\underline{\beta},\bar{\beta}}(\hat{\beta}_2), \cdots, \mathrm{sat}_{\underline{\beta},\bar{\beta}}(\hat{\beta}_m)\big]^T$.

IV. CONVERGENCE ANALYSIS

Theorem 1: For the closed-loop PAM ILC system composed of (8) and (17)-(20), the tracking performance and system stability are guaranteed as follows:

(i) $\lim_{k\to\infty}\|\boldsymbol{e}_k(t)\| = 0$ holds for $t \in [t_\omega, T]$;

(ii) $|s_{r,k}(t)| < b_s$ holds during each iteration for $t \in [0, T]$.

(iii) All adjustable control parameters and internal signals are bounded $\forall t \in [0, T]$, $\forall k$.

Proof 1: Define a barrier Lyapunov functional as follows:

$$\begin{aligned}L_k = V_k + \frac{g}{2\gamma_2}\int_0^t \tilde{\boldsymbol{\varpi}}_k^T\tilde{\boldsymbol{\varpi}}_k d\tau + \frac{g}{2\gamma_3}\int_0^t \tilde{\boldsymbol{w}}_k^T\tilde{\boldsymbol{w}}_k d\tau \\ + \frac{g}{2\gamma_4}\int_0^t \tilde{\epsilon}_{N,k}^2 d\tau,\end{aligned} \tag{21}$$

where $\tilde{\boldsymbol{\varpi}}_k = \boldsymbol{\varpi} - \boldsymbol{\varpi}_k$, $\tilde{\boldsymbol{w}}_k = \boldsymbol{w}^* - \boldsymbol{w}_k$ and $\tilde{\epsilon}_{N,k} = \epsilon_N - \epsilon_{N,k}$.

part A In this part, we will give the detailed calculation process of $L_k - L_{k-1}$ for subsequent analysis.

While $k > 0$, according to the definition of L_k, we obtain

$$\begin{aligned}L_k - L_{k-1} &= V_k - V_{k-1} + \frac{g}{2\gamma_2}\int_0^t(\tilde{\boldsymbol{\varpi}}_k^T\tilde{\boldsymbol{\varpi}}_k - \tilde{\boldsymbol{\varpi}}_{k-1}^T\tilde{\boldsymbol{\varpi}}_{k-1})d\tau \\ &\quad + \frac{g}{2\gamma_3}\int_0^t(\tilde{\boldsymbol{w}}_k^T\tilde{\boldsymbol{w}}_k - \tilde{\boldsymbol{w}}_{k-1}^T\tilde{\boldsymbol{w}}_{k-1})d\tau \\ &\quad + \frac{g}{2\gamma_4}\int_0^t(\tilde{\epsilon}_{N,k}^2 - \tilde{\epsilon}_{N,k-1}^2)d\tau.\end{aligned} \tag{22}$$

Combining (17) with (16) yields

$$\begin{aligned}\dot{V}_k \le -\gamma\sigma_k g s_{r,k}^2 + \sigma_k s_{r,k} g\tilde{\boldsymbol{\varpi}}_k^T\boldsymbol{\xi}_k + \sigma_k s_{r,k} g\tilde{\boldsymbol{w}}_k^T(t)\boldsymbol{\varphi}(\boldsymbol{x}_k) \\ + \sigma_k s_{r,k} g\tilde{\epsilon}_{N,k} + \sigma_k s_{r,k} g\epsilon_{N,k} - \sigma_k s_{r,k} g\epsilon_{N,k}\tanh(\sigma_k s_{r,k} \\ \times \epsilon_{N,k}(k+1)^2),\end{aligned} \tag{23}$$

By the property $0 \le |\alpha| - \alpha\tanh(\frac{\alpha}{\varepsilon}) \le 0.2785\varepsilon$, we obtain

$$\begin{aligned}\sigma_k s_{r,k} g\epsilon_{N,k} - \sigma_k s_{r,k} g\epsilon_{N,k}\tanh(\sigma_k s_{r,k}\epsilon_{N,k}(k+1)^2) \\ \le \frac{0.2785g}{(k+1)^2}.\end{aligned} \tag{24}$$

Note that $V_k(0) = 0$ holds because $s_{r,k}(0) = 0$ is guaranteed according to the construction strategy of $\boldsymbol{e}_{r,k}(t)$. Based on (23) and (24), calculating the integral of $\dot{V}_k$ from 0 to t, we have

$$\begin{aligned}V_k \le -\gamma_1 g\int_0^t \sigma_k s_{r,k}^2 d\tau + \int_0^t \sigma_k s_{r,k} g\tilde{\boldsymbol{\varpi}}_k^T\boldsymbol{\xi}_k d\tau \\ + \int_0^t g\sigma_k s_{r,k}\tilde{\boldsymbol{w}}_k^T\boldsymbol{\varphi}_k d\tau + \int_0^t g\sigma_k|s_{r,k}|\tilde{\epsilon}_{N,k}d\tau \\ + \frac{0.2785gt}{(k+1)^2}.\end{aligned} \tag{25}$$

Then, substituting (25) into (22), we get

$$\begin{aligned}L_k - L_{k-1} \le -\gamma_1 g\int_0^t \sigma_k s_{r,k}^2 d\tau + \int_0^t \sigma_k s_{r,k} g\tilde{\boldsymbol{\varpi}}_k^T\boldsymbol{\xi}_k d\tau \\ + \int_0^t g\sigma_k s_{r,k}\tilde{\boldsymbol{w}}_k^T\boldsymbol{\varphi}_k d\tau + \int_0^t g\sigma_k|s_{r,k}|\tilde{\epsilon}_{N,k}d\tau \\ - V_{k-1} + \frac{g}{2\gamma_2}\int_0^t(\tilde{\boldsymbol{\varpi}}_k^T\tilde{\boldsymbol{\varpi}}_k - \tilde{\boldsymbol{\varpi}}_{k-1}^T\tilde{\boldsymbol{\varpi}}_{k-1})d\tau\end{aligned}$$

$$+\frac{0.2785gt}{(k+1)^2}+\frac{g}{2\gamma_3}\int_0^t(\tilde{\boldsymbol{w}}_k^T\tilde{\boldsymbol{w}}_k-\tilde{\boldsymbol{w}}_{k-1}^T\tilde{\boldsymbol{w}}_{k-1})d\tau+\frac{g}{2\gamma_4}\int_0^t(\tilde{\epsilon}_{N,k}^2-\tilde{\epsilon}_{N,k-1}^2)d\tau. \tag{26}$$

From (18), we obtain

$$\begin{aligned}&\frac{g}{2\gamma_2}(\tilde{\boldsymbol{\varpi}}_k^T\tilde{\boldsymbol{\varpi}}_k-\tilde{\boldsymbol{\varpi}}_{k-1}^T\tilde{\boldsymbol{\varpi}}_{k-1})+g\sigma_k s_{\phi,k}\tilde{\boldsymbol{\varpi}}_k^T\boldsymbol{\xi}_k\\&\le\frac{g}{2\gamma_2}[(\boldsymbol{\varpi}-\boldsymbol{\varpi}_k)^T(\boldsymbol{\varpi}-\boldsymbol{\varpi}_k)-(\boldsymbol{\varpi}-\mathrm{sat}_{\underline{\varpi},\bar{\varpi}}(\boldsymbol{\varpi}_{k-1}))^T(\boldsymbol{\varpi}\\&\quad-\mathrm{sat}_{\underline{\varpi},\bar{\varpi}}(\boldsymbol{\varpi}_{k-1}))]+g\sigma_k s_{\phi,k}\tilde{\boldsymbol{\varpi}}_k^T\boldsymbol{\xi}_k\\&\le\frac{g}{2\gamma_2}(2\boldsymbol{\varpi}-\boldsymbol{\varpi}_k-\mathrm{sat}_{\underline{\varpi},\bar{\varpi}}(\boldsymbol{\varpi}_{k-1}))^T(\mathrm{sat}_{\underline{\varpi},\bar{\varpi}}(\boldsymbol{\varpi}_{k-1})-\boldsymbol{\varpi}_k)\\&\quad+g\sigma_k s_{\phi,k}\tilde{\boldsymbol{\varpi}}_k^T\boldsymbol{\xi}_k\\&\le\frac{g}{\gamma_2}(\boldsymbol{\varpi}-\boldsymbol{\varpi}_k)^T[\mathrm{sat}_{\underline{\varpi},\bar{\varpi}}(\boldsymbol{\varpi}_{k-1})-\boldsymbol{\varpi}_k+\gamma_2\sigma_k s_{\phi,k}\boldsymbol{\xi}_k]\\&=0.\end{aligned} \tag{27}$$

Combining (27) with (28), we have

$$\begin{aligned}L_k-L_{k-1}\le&-\gamma_1 g\int_0^t\sigma_k s_{r,k}^2d\tau+\int_0^t g\sigma_k s_{r,k}\tilde{\boldsymbol{w}}_k^T\boldsymbol{\varphi}_k d\tau\\&+\frac{0.2785gt}{(k+1)^2}+\int_0^t g\sigma_k|s_{r,k}|\tilde{\epsilon}_{N,k}d\tau-V_{k-1}\\&+\frac{g}{2\gamma_3}\int_0^t(\tilde{\boldsymbol{w}}_k^T\tilde{\boldsymbol{w}}_k-\tilde{\boldsymbol{w}}_{k-1}^T\tilde{\boldsymbol{w}}_{k-1})d\tau\\&+\frac{g}{2\gamma_4}\int_0^t(\tilde{\epsilon}_{N,k}^2-\tilde{\epsilon}_{N,k-1}^2)d\tau.\end{aligned} \tag{28}$$

From (19), we have

$$\begin{aligned}&\frac{g}{2\gamma_3}(\tilde{\boldsymbol{w}}_k^T\tilde{\boldsymbol{w}}_k-\tilde{\boldsymbol{w}}_{k-1}^T\tilde{\boldsymbol{w}}_{k-1})+g\sigma_k s_{\phi,k}\tilde{\boldsymbol{w}}_k^T\boldsymbol{\varphi}_k\\&\le\frac{g}{2\gamma_3}[(\boldsymbol{w}^*-\boldsymbol{w}_k)^T(\boldsymbol{w}^*-\boldsymbol{w}_k)-(\boldsymbol{w}^*-\mathrm{sat}_{\underline{w},\bar{w}}(\boldsymbol{w}_{k-1}))^T(\boldsymbol{w}^*\\&\quad-\mathrm{sat}_{\underline{w},\bar{w}}(\boldsymbol{w}_{k-1}))]+g\sigma_k s_{\phi,k}\tilde{\boldsymbol{w}}_k^T\boldsymbol{\varphi}_k\\&\le\frac{g}{2\gamma_3}(2\boldsymbol{w}^*-\boldsymbol{w}_k-\mathrm{sat}_{\underline{w},\bar{w}}(\boldsymbol{w}_{k-1}))^T(\mathrm{sat}_{\underline{w},\bar{w}}(\boldsymbol{w}_{k-1})-\boldsymbol{w}_k)\\&\quad+g\sigma_k s_{\phi,k}\tilde{\boldsymbol{w}}_k^T\boldsymbol{\varphi}_k\\&\le\frac{g}{\gamma_3}(\boldsymbol{w}^*-\boldsymbol{w}_k)^T[\mathrm{sat}_{\underline{w},\bar{w}}(\boldsymbol{w}_{k-1})-\boldsymbol{w}_k+\gamma_3\sigma_k s_{\phi,k}\boldsymbol{\varphi}_k]\\&=0.\end{aligned} \tag{29}$$

Similarly, from (20), we get

$$\begin{aligned}&\frac{g}{2\gamma_4}(\tilde{\epsilon}_{N,k}^2-\tilde{\epsilon}_{N,k-1}^2)+g\sigma_k|s_{r,k}|\tilde{\epsilon}_{N,k}\\&\le\frac{g}{\gamma_4}(\epsilon_N-\epsilon_{N,k})\big[\mathrm{sat}_{0,\bar{\epsilon}_N}(\epsilon_{N,k-1})-\epsilon_{N,k}+\gamma_4 g\sigma_k|s_{r,k}|\big]\\&=0.\end{aligned} \tag{30}$$

It follows from the above three inequations that

$$L_k-L_{k-1}\le-V_{k-1}+\frac{0.2785gt}{(k+1)^2}. \tag{31}$$

Note that $\lim_{k\to\infty}\sum_{j=1}^{j=k+1}\frac{0.2785gt}{j^2}=\frac{0.2785\pi^2gt}{3}$ holds. Further, we can get the recursive result of (31) as

$$L_k(t)\le L_0(t)+\frac{0.2785\pi^2gt}{3}-\frac{1}{2}\sum_{j=0}^{k-1}\frac{s_{r,k}^2}{b_s^2-s_{r,k}^2}. \tag{32}$$

part B In this part, we will prove that $b_s^2-s_{r,k}^2(t)>0,\forall k$, for $t\in[0,T]$.

From (21)-(24), we have

$$\begin{aligned}\dot{L}_k\le&-\gamma\sigma_k g s_{r,k}^2+\sigma_k s_{r,k}g\tilde{\boldsymbol{\varpi}}_k^T\boldsymbol{\xi}_k+\sigma_k s_{r,k}g\tilde{\boldsymbol{w}}_k^T\boldsymbol{\varphi}_k\\&+\sigma_k s_{r,k}g\tilde{\epsilon}_{N,k}+\frac{0.2785g}{(k+1)^2}+\frac{g}{2\gamma_2}\tilde{\boldsymbol{\eta}}_k^T\tilde{\boldsymbol{\eta}}_k+\frac{g}{2\gamma_3}\tilde{\boldsymbol{w}}_k^T\tilde{\boldsymbol{w}}_k\\&+\frac{g}{2\gamma_4}\tilde{\epsilon}_{N,k}^2.\end{aligned} \tag{33}$$

By the property of saturation function and (18), we have

$$\begin{aligned}&\sigma_k s_{r,k}g\tilde{\boldsymbol{\varpi}}_k^T\boldsymbol{\xi}_k+\frac{1}{2\gamma_2}g\tilde{\boldsymbol{\varpi}}_k^T\tilde{\boldsymbol{\varpi}}_k\\&=\frac{g}{2\gamma_2}(\boldsymbol{\varpi}-\boldsymbol{\varpi}_k)^T(2\boldsymbol{\varpi}_k-2\mathrm{sat}_{\underline{\varpi},\bar{\varpi}}(\boldsymbol{\varpi}_{k-1})+\boldsymbol{\varpi}-\boldsymbol{\varpi}_k)\\&=\frac{g}{2\gamma_2}[-\boldsymbol{\varpi}_k^T\boldsymbol{\varpi}_k+\boldsymbol{\varpi}^T\boldsymbol{\varpi}-2\boldsymbol{\varpi}^T\mathrm{sat}_{\underline{\varpi},\bar{\varpi}}(\boldsymbol{\varpi}_{k-1})\\&\quad+2\boldsymbol{\varpi}_k^T\mathrm{sat}_{\underline{\varpi},\bar{\varpi}}(\boldsymbol{\varpi}_{k-1})]\\&=-\frac{g}{2\gamma_2}[\boldsymbol{\varpi}_k-\mathrm{sat}_{\underline{\varpi},\bar{\varpi}}(\boldsymbol{\varpi}_{k-1})]^T[\boldsymbol{\varpi}_k-\mathrm{sat}_{\underline{\varpi},\bar{\varpi}}(\boldsymbol{\varpi}_{k-1})]\\&\quad+\frac{g}{2\gamma_2}[\mathrm{sat}_{\underline{\varpi},\bar{\varpi}}(\boldsymbol{\varpi}_{k-1}^T)\mathrm{sat}_{\underline{\varpi},\bar{\varpi}}(\boldsymbol{\varpi}_{k-1})+\boldsymbol{\varpi}^T\boldsymbol{\varpi}\\&\quad-2\boldsymbol{\varpi}^T\mathrm{sat}_{\underline{\varpi},\bar{\varpi}}(\boldsymbol{\varpi}_{k-1})]\\&\le\frac{g}{2\gamma_2}[\mathrm{sat}_{\underline{\varpi},\bar{\varpi}}(\boldsymbol{\varpi}_{k-1}^T)\mathrm{sat}_{\underline{\varpi},\bar{\varpi}}(\boldsymbol{\varpi}_{k-1})+\boldsymbol{\varpi}^T\boldsymbol{\varpi}\\&\quad-2\boldsymbol{\varpi}^T\mathrm{sat}_{\underline{\varpi},\bar{\varpi}}(\boldsymbol{\varpi}_{k-1})]\\&\le m_{\varpi},\end{aligned} \tag{34}$$

in which m_{ϖ} is a proper positive number. Similarly, for a large enough $m_w>0$, by using the learning law (19), we obtain

$$\begin{aligned}&\sigma_k s_{r,k}g\tilde{\boldsymbol{w}}_k^T\boldsymbol{\varphi}_k+\frac{g}{2\gamma_2}\tilde{\boldsymbol{w}}_k^T\tilde{\boldsymbol{w}}_k\\&=\frac{g}{2\gamma_2}[-\boldsymbol{w}_k^T\boldsymbol{w}_k+\boldsymbol{w}^{*T}\boldsymbol{w}^*-2\boldsymbol{w}^{*T}\mathrm{sat}_{\underline{w},\bar{w}}(\boldsymbol{w}_{k-1})\\&\quad+2\boldsymbol{w}_k^T\mathrm{sat}_{\underline{w},\bar{w}}(\boldsymbol{w}_{k-1})]\\&=-\frac{g}{2\gamma_2}[\boldsymbol{w}_k-\mathrm{sat}_{\underline{w},\bar{w}}(\boldsymbol{w}_{k-1})]^T[\boldsymbol{w}_k-\mathrm{sat}_{\underline{w},\bar{w}}(\boldsymbol{w}_{k-1})]\\&\quad+\frac{g}{2\gamma_2}[\mathrm{sat}_{\underline{w},\bar{w}}(\boldsymbol{w}_{k-1}^{*T})\mathrm{sat}_{\underline{w},\bar{w}}(\boldsymbol{w}_{k-1})+\boldsymbol{w}^{*T}\boldsymbol{w}^*\\&\quad-2\boldsymbol{w}^{*T}\mathrm{sat}_{\underline{w},\bar{w}}(\boldsymbol{w}_{k-1})]\\&\le\frac{g}{2\gamma_2}[\mathrm{sat}_{\underline{w},\bar{w}}(\boldsymbol{w}_{k-1}^{*T})\mathrm{sat}_{\underline{w},\bar{w}}(\boldsymbol{w}_{k-1})+\boldsymbol{w}^{*T}\boldsymbol{w}^*\\&\quad-2\boldsymbol{w}^{*T}\mathrm{sat}_{\underline{w},\bar{w}}(\boldsymbol{w}_{k-1})]\\&\le m_w.\end{aligned} \tag{35}$$

For a large enough $m_\epsilon>0$, with the help of the learning law (20), we have

$$\begin{aligned}&\sigma_k|s_{r,k}|\tilde{\epsilon}_{N,k}+\frac{1}{2\gamma_5}\tilde{\epsilon}_{N,k}^2\\&=\frac{1}{2\gamma_5}[-\epsilon_{N,k}^2+\epsilon_N^2-2\epsilon_N\mathrm{sat}_{0,\bar{\epsilon}}(\epsilon_{N,k-1})\\&\quad+2\epsilon_k\mathrm{sat}_{0,\bar{\epsilon}_N}(\epsilon_{N,k-1})]\\&=\frac{1}{2\gamma_5}[\mathrm{sat}_{0,\bar{\epsilon}_N}(\epsilon_{N,k-1})\mathrm{sat}_{0,\bar{\epsilon}}(\epsilon_{N,k-1})+\epsilon_N^2\end{aligned}$$

$$
\begin{aligned}
&- 2\epsilon_N \mathrm{sat}_{0,\bar{\epsilon}_N}(\epsilon_{N,k-1})] \\
&- \frac{1}{2\gamma_5}[\epsilon_{N,k} - \mathrm{sat}_{0,\bar{\epsilon}_N}(\epsilon_{N,k-1})]^2 \\
&\le \frac{1}{2\gamma_5}[\mathrm{sat}_{0,\bar{\epsilon}_N}(\epsilon_{k-1})\mathrm{sat}_{0,\bar{\epsilon}_N}(\epsilon_{N,k-1}) + \epsilon_N^2 - 2\epsilon_N \\
&\quad \times \mathrm{sat}_{0,\bar{\epsilon}_N}(\epsilon_{N,k-1})] \\
&\le m_\epsilon. \qquad (36)
\end{aligned}
$$

Substituting (34)-(36) into (33) yields

$$\dot{L}_k \le \frac{0.2785g}{(k+1)^2} + m_\varpi + m_w + m_\epsilon. \qquad (37)$$

On the basis of which and $L_k(0) = 0$, we get

$$L_k(t) \le \frac{0.2785gt}{(k+1)^2} + t(m_\varpi + m_w + m_\epsilon). \qquad (38)$$

According to the definition of $L_k(t)$, we then deduce

$$V_k(t) = \frac{s_{r,k}^2(t)}{2(b_s^2 - s_{r,k}^2(t))} \le \frac{0.2785gt}{(k+1)^2} + t(m_\varpi + m_w + m_\epsilon) \qquad (39)$$

holds during each iteration for $t \in [0, T]$. Note that $s_{r,k}^2(0) = 0$ for any $k \ge 0$. Suppose that $|s_{r,k}(t)|$ may increase to b_{s-} for any $t \in (0, T]$, then

$$V_k(t) = \frac{s_{r,k}^2(t)}{2(b_s^2 - s_{r,k}^2(t))} \to +\infty \qquad (40)$$

would happen, which is contrary to the inequality (39). Therefore,

$$|s_{r,k}(t)| < b_{s-} \qquad (41)$$

holds during each iteration. By Using the relationship $\lambda e_{r1,k} + \dot{e}_{r1,k} = s_{r,k}$, from (41), we can obtain

$$
\begin{aligned}
|e_{r1,k}(t)| &< \mathrm{e}^{-\lambda t}|e_{r1,k}(0)| + \frac{(1 - \mathrm{e}^{-\lambda t})b_s}{\lambda} \\
&= \frac{(1 - \mathrm{e}^{-\lambda t})b_s}{\lambda}. \qquad (42)
\end{aligned}
$$

On the other hand, according to (41), the boundedness of $e_{r1,k}$, $e_{r2,k}$, $x_{r1,k}$ and $x_{r2,k}$ may be deduced. Then, from (18)-(20), we can check that $\boldsymbol{\varpi}_k$, $\boldsymbol{w}_k$ and ϵ_k are bounded. Further, u_k and all other signals in the closed-loop system may be verified to be bounded.

part C In this part, we will analyze the convergence of tracking error.

It is a direct result of (38) that

$$L_0(t) \le 0.2785gt + t(m_\varpi + m_w + m_\epsilon). \qquad (43)$$

Applying the conclusion given in (43), we have

$$
\begin{aligned}
L_k(t) &\le 0.2785gt + t(m_\varpi + m_w + m_\epsilon) + \frac{0.2785\pi^2 gt}{3} \\
&\quad - \frac{1}{2}\sum_{j=0}^{k-1} \frac{s_{r,k}^2}{b_s^2 - s_{r,k}^2} \\
&\le 0.2785gt + t(m_\varpi + m_w + m_\epsilon) + \frac{0.2785\pi^2 gt}{3} \\
&\quad - \frac{1}{2b_s^2}\sum_{j=0}^{k-1} s_{r,k}^2. \qquad (44)
\end{aligned}
$$

By using the nonnegativity of $L_k(t)$, (44) means

$$
\begin{aligned}
&0.2785gt + t(m_\varpi + m_w + m_\epsilon) + \frac{0.2785\pi^2 gt}{3} \\
&\quad - \frac{1}{2b_s^2}\sum_{j=0}^{k-1} s_{r,k}^2(t) \ge 0. \qquad (45)
\end{aligned}
$$

From (45), we have

$$\lim_{k \to +\infty} |s_{r,k}(t)| = 0. \qquad (46)$$

Considering the fact that $ce_{r1,k} + \dot{e}_{r1,k} = s_{r,k}$, $e_{r1,k}(0) = 0$ and $\dot{e}_{r1,k}(0) = 0$ hold, from (46), we can see that

TABLE 1. Parameters of PAM system.

Parameters			
$c_0 = 0.9$	$c_1 = 1$	$c_2 = 1.5$	$c_3 = 4$
$c_u = 1$	$\epsilon_0 = 0.5$	$b_p = 2$	$r = 4$cm
$l_0 = 20$cm	$u_o = 0.5V$	$J_p = 10\ \mathrm{kg \cdot cm}$	

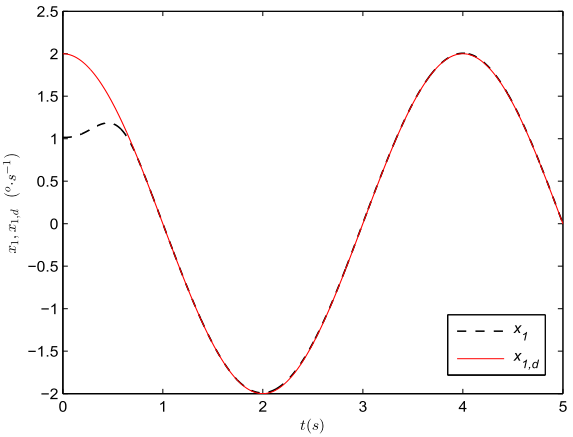

FIGURE 2. x_1 and its reference signal $x_{1,d}$ ($k = 29$).

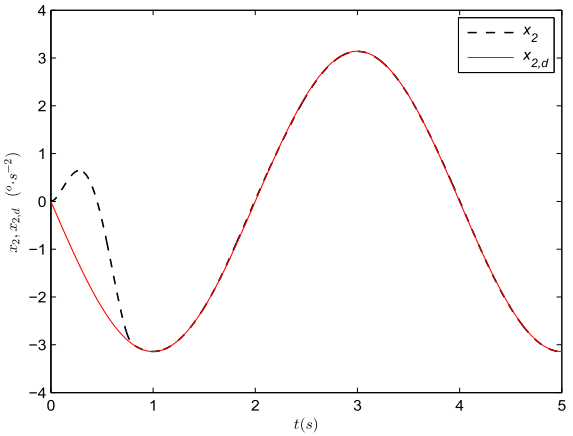

FIGURE 3. x_2 and its reference signal $x_{2,d}$ ($k = 29$).

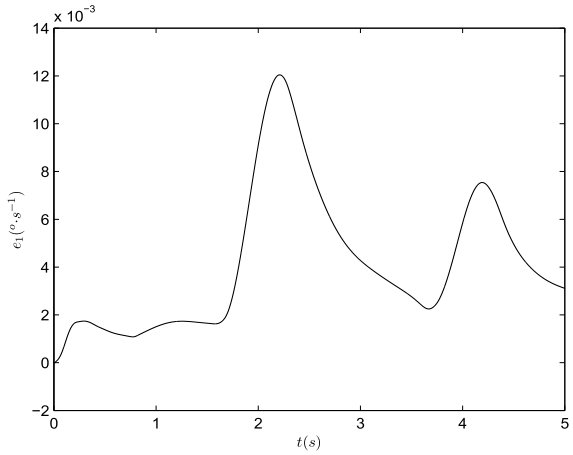

FIGURE 4. The error e_1 ($k = 29$).

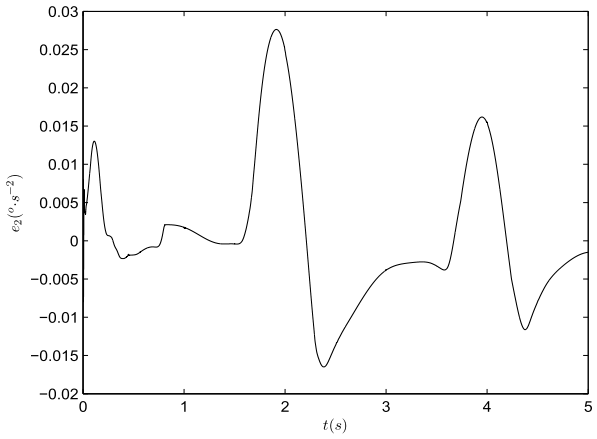

FIGURE 5. The error e_2 ($k = 29$).

$\lim_{k\to+\infty}|e_{r1,k}(t)| = 0$ and $\lim_{k\to+\infty}|e_{r2,k}(t)| = 0$ hold, which implies $\lim_{k\to\infty}\|\boldsymbol{e}_k(t)\| = 0$ holds for $t \in [t_\omega, T]$.

In this work, barrier Lyapunov function approach is used to design the iterative learning controller. Through constraining $s_{r,k}$, we implement the constraint to $e_{r1,k}$ and $e_{r2,k}$ during each iteration.

V. NUMERICAL SIMULATION

The numerical simulation is performed for the PAM system (8), where $d_{p,k} = 3 + 2\text{rand}_1 + 1.5x_{1,k}^2 + x_{1,k}x_{2,k} + 0.5\sin(x_{1,k})x_{2,k} + 0.1\text{sgn}(x_{1,k}x_{2,k})$, $[x_{1,k}(0), x_{2,k}(0) = [1 + 0.1\text{rand}_2, 0.05\text{rand}_3]^T$ and the model parameters are listed in TABLE 1. Here, $\text{rand}_1 - \text{rand}_3$ are random numbers between 0 and 1.

The reference position trajectories is set as

$$y_d(t) = \begin{cases} 0.5\cos(\pi t) & k = 0, 2, 4, 6, \cdots \\ 1.6\cos(\frac{\pi}{2}t) & k = 1, 3, 5, 7, \cdots \end{cases} \quad (47)$$

The parameters of RBF network neurons in (15) are set as follows: $b_j = 3.5$ and c_j is evenly spaced on $[-3, 3]\times[-3, 3]$, for $j = 1, 2, \cdots, m$, $m = 7$. The control parameters and gains in control law (17) and learning laws (18)-(19) are set as follows: $\lambda = 2, \gamma_1 = 5, \gamma_2 = 1, \gamma_3 = 1, \gamma_4 = 0.1$, $b_s = 0.2, t_\omega = 0.8s, T = 5s$.

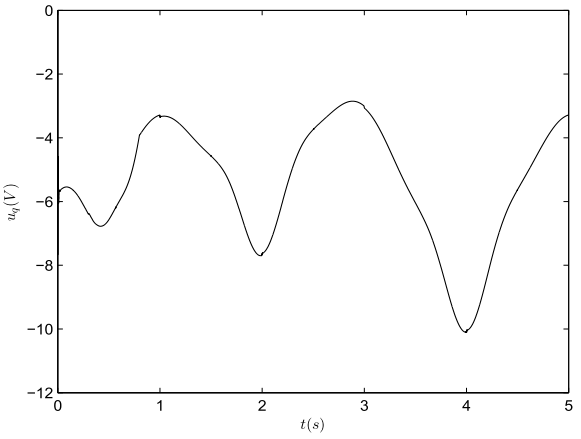

FIGURE 6. Control input ($k = 29$).

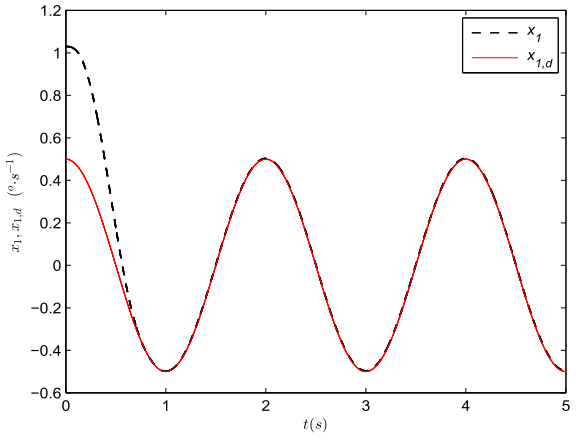

FIGURE 7. x_1 and its reference signal $x_{1,d}$ ($k = 30$).

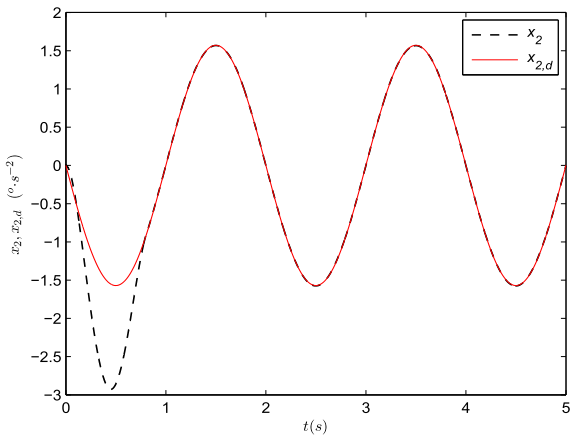

FIGURE 8. x_2 and its reference signal $x_{2,d}$ ($k = 30$).

Figs. 2-12 express the simulation results. Figs. 2-3 give the profiles of angle position/angular velocity x_1 and their reference signals $x_{1,d}$ and $x_{2,d}$ during 29th iteration, respectively. Figs. 4-5 show the curves of e_{r1} and e_{r2} during 29th iteration, respectively. The control signal $u_q(t)$ during 29th iteration is depicted in Fig. 6. Figs. 7-8 give the profiles of angle position/angular velocity x_1 and their reference signals $x_{1,d}$ and $x_{2,d}$ during 30th iteration, respectively. Figs. 9-10 show the curves of e_{r1} and e_{r2} during 30th

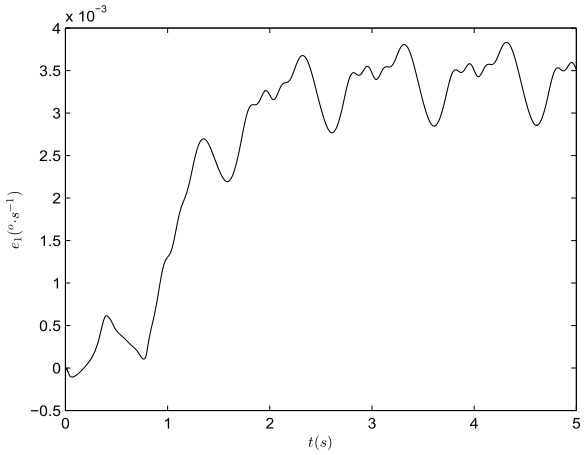

FIGURE 9. The error e_1 ($k = 30$).

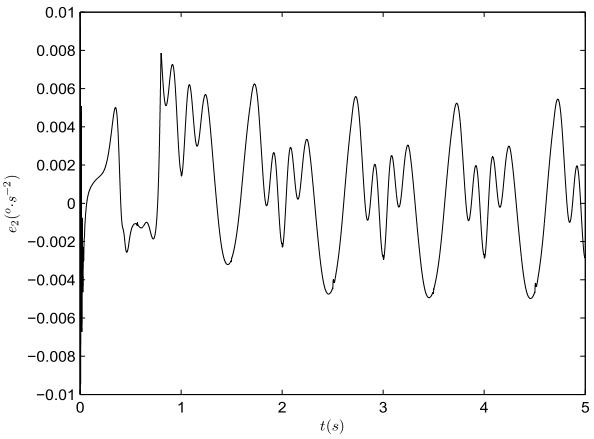

FIGURE 10. The error e_2 ($k = 30$).

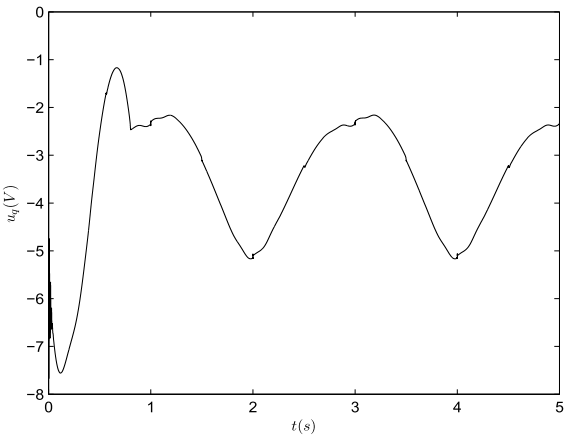

FIGURE 11. Control input ($k = 30$).

iteration, respectively. The control signal $u_q(t)$ during 30th iteration is depicted in Fig. 11. From Figs. 2-3 and Figs. 7-8, we can see that angle position/angular velocity states can accurately the reference signals for $t \in [t_\omega, T]$, respectively. As shown in Figs. 4-5 and Figs. 9-10, the rectification state error converges to zero over the interval $[0, T]$ as the iteration number increases. It can be observed from Fig. 12 that $s_{r,k}$ converges to zero, and $|s_{r,k}|$ is constrained between 0 and

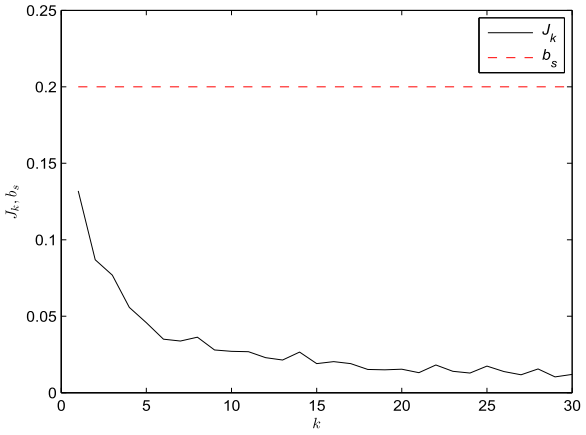

FIGURE 12. History of $s_{r,k}$ convergence.

b_s during each iteration, where $J_k \triangleq \max_{t\in[0,T]} |s_{r,k}|$. The above simulation results show that the tracking performance of closed-loop PAM ILC system improves progressively as the iteration number increases.

VI. CONCLUSION

An initial-rectification adaptive ILC scheme is proposed for a PAM system with nonzero initial errors and iteration-varying reference trajectories. The iterative learning controller is developed by using barrier Lyapunov function approach so as to constraint rectification filtering error during each iteration. A new initial rectification construction method is given to solve the nonzero initial error problem of PAM ILC system. The nonparametric uncertainties in the system are approximated by using a difference-learning neural network. As the iteration number increases, the system state can accurately track the reference trajectory over the whole interval, even if the reference trajectories are non-repetitive over the iteration domain.

REFERENCES

[1] S. Q. Xie and P. K. Jamwal, "An iterative fuzzy controller for pneumatic muscle driven rehabilitation robot," *Expert Syst. Appl.*, vol. 38, no. 7, pp. 8128–8137, Jul. 2011.

[2] N. Sun, D. Liang, Y. Wu, Y. Chen, Y. Qin, and Y. Fang, "Adaptive control for pneumatic artificial muscle systems with parametric uncertainties and unidirectional input constraints," *IEEE Trans. Ind. Informat.*, vol. 16, no. 2, pp. 969–979, Feb. 2020.

[3] M. Sugisaka and H. Zhao, "The characteristics of McKibben muscle based on the pneumatic experiment system," *Artif. Life Robot.*, vol. 11, no. 2, pp. 223–226, Jul. 2007.

[4] H. Yang, Y. Yu, and J. Zhang, "Angle tracking of a pneumatic muscle actuator mechanism under varying load conditions," *Control Eng. Pract.*, vol. 61, pp. 1–10, Apr. 2017.

[5] L. Zhao, H. Cheng, J. Zhang, and Y. Xia, "Angle attitude control for a 2-DOF parallel mechanism of PMAs using tracking differentiators," *IEEE Trans. Ind. Electron.*, vol. 66, no. 11, pp. 8659–8669, Nov. 2019.

[6] G. Andrikopoulos, G. Nikolakopoulos, and S. Manesis, "Advanced nonlinear PID-based antagonistic control for pneumatic muscle actuators," *IEEE Trans. Ind. Electron.*, vol. 61, no. 12, pp. 6926–6937, Dec. 2014.

[7] H. Aschemann and D. Schindele, "Sliding-mode control of a high-speed linear axis driven by pneumatic muscle actuators," *IEEE Trans. Ind. Electron.*, vol. 55, no. 11, pp. 3855–3864, Nov. 2008.

[8] K. Xing, Q. Xu, J. Huang, Y. Wang, J. He, and J. Wu, "Tracking control of pneumatic artificial muscle actuators based on sliding mode and non-linear disturbance observer," *IET Control Theory Appl.*, vol. 4, no. 10, pp. 2058–2070, Oct. 2010.

[9] J.-P. Cai, F. Qian, R. Yu, and L. Shen, "Adaptive control for a pneumatic muscle joint system with saturation input," *IEEE Access*, vol. 8, pp. 117698–117705, 2020.
[10] J. Huang, J. Qian, L. Liu, Y. Wang, C. Xiong, and S. Ri, "Echo state network based predictive control with particle swarm optimization for pneumatic muscle actuator," *J. Franklin Inst.*, vol. 353, no. 12, pp. 2761–2782, Aug. 2016.
[11] L. Zhao, H. Cheng, Y. Xia, and B. Liu, "Angle tracking adaptive backstepping control for a mechanism of pneumatic muscle actuators via an AESO," *IEEE Trans. Ind. Electron.*, vol. 66, no. 6, pp. 4566–4576, Jun. 2019.
[12] Y. Yuan, Y. Yu, and L. Guo, "Nonlinear active disturbance rejection control for the pneumatic muscle actuators with discrete-time measurements," *IEEE Trans. Ind. Electron.*, vol. 66, no. 3, pp. 2044–2053, Mar. 2019.
[13] D. Meng and J. Zhang, "Robust optimization-based iterative learning control for nonlinear systems with nonrepetitive uncertainties," *IEEE/CAA J. Automatica Sinica*, vol. 8, no. 5, pp. 1001–1014, May 2021.
[14] D. Shen, "Iterative learning control with incomplete information: A survey," *IEEE/CAA J. Automatica Sinica*, vol. 5, no. 5, pp. 885–901, Jul. 2018.
[15] J. Liu, X. Ruan, and Y. Zheng, "Iterative learning control for discrete-time systems with full learnability," *IEEE Trans. Neural Netw. Learn. Syst.*, vol. 33, no. 2, pp. 629–643, Feb. 2022.
[16] Y. Wang, E. Dassau, and F. Doyle, "Closed-loop control of artificial pancreatic η-cell in type 1 diabetes mellitus using model predictive iterative learning control," *IEEE Trans. Biomed. Eng.*, vol. 57, no. 2, pp. 211–219, Feb. 2010.
[17] X. Li, J.-X. Xu, and D. Huang, "An iterative learning control approach for linear systems with randomly varying trial lengths," *IEEE Trans. Autom. Control*, vol. 59, no. 7, pp. 1954–1960, Jul. 2014.
[18] X. Bu, Q. Yu, Z. Hou, and W. Qian, "Model free adaptive iterative learning consensus tracking control for a class of nonlinear multiagent systems," *IEEE Trans. Syst., Man, Cybern., Syst.*, vol. 49, no. 4, pp. 677–686, Apr. 2019.
[19] G. Li, Y. Han, T. Lu, D. Chen, and H. Chen, "Iterative learning control for nonlinear multi-agent systems with initial shifts," *IEEE Access*, vol. 8, pp. 144343–144351, 2020.
[20] Y. Yu, J. Wan, and H. Bi, "Suboptimal learning control for nonlinearly parametric time-delay systems under alignment condition," *IEEE Access*, vol. 6, pp. 2922–2929, 2018.
[21] X. Dai and X. Zhou, "Mixed PD-type iterative learning control algorithm for a class of parabolic singular distributed parameter systems," *IEEE Access*, vol. 9, pp. 12180–12190, 2021.
[22] W. Cao, J. Qiao, and M. Sun, "Consensus control via iterative learning for singular multi-agent systems with switching topologies," *IEEE Access*, vol. 9, pp. 81412–81420, 2021.
[23] T. Hu, K. H. Low, L. Shen, and X. Xu, "Effective phase tracking for bioinspired undulations of robotic fish models: A learning control approach," *IEEE/ASME Trans. Mechatronics*, vol. 19, no. 1, pp. 191–200, Feb. 2014.
[24] B. Jia, S. Liu, and Y. Liu, "Visual trajectory tracking of industrial manipulator with iterative learning control," *Ind. Robot, Int. J.*, vol. 42, no. 1, pp. 54–63, Jan. 2015.
[25] D. Huang, W. Yang, T. Huang, N. Qin, Y. Chen, and Y. Tan, "Iterative learning operation control of high-speed trains with adhesion dynamics," *IEEE Trans. Control Syst. Technol.*, vol. 29, no. 6, pp. 2598–2608, Nov. 2021.
[26] D. Guo, W. Wang, Y. Zhang, Q. Yan, and J. Cai, "Angle tracking robust learning control for pneumatic artificial muscle systems," *IEEE Access*, vol. 9, pp. 142232–142238, 2021.
[27] Q. Yang, W. Wang, Y. Zhang, Q. Yan, and J. Cai, "Angle error-tracking iterative learning control for pneumatic artificial muscle system," *IEEE Access*, vol. 9, pp. 163099–163107, 2021.
[28] S. Saab, W. Vogt, and M. Mickle, "Learning control algorithms for tracking 'slowly' varying trajectories," *IEEE Trans. Syst., Man, Cybern., B, Cybern.*, vol. 27, no. 4, pp. 657–670, Aug. 1997.
[29] J.-X. Xu and J. Xu, "On iterative learning from different tracking tasks in the presence of time-varying uncertainties," *IEEE Trans. Syst., Man, Cybern., B, Cybern.*, vol. 34, no. 1, pp. 589–597, Feb. 2004.
[30] C.-J. Chien, "A combined adaptive law for fuzzy iterative learning control of nonlinear systems with varying control tasks," *IEEE Trans. Fuzzy Syst.*, vol. 16, no. 1, pp. 40–51, Feb. 2008.
[31] J.-M. Li, Y.-P. Sun, and Y. Liu, "Hybrid adaptive iterative learning control of non-uniform trajectory tracking," *Control Theory Appl.*, vol. 25, no. 1, pp. 100–104, Jan. 2008.
[32] R. Chi, Z. Hou, and J.-X. Xu, "Adaptive ILC for a class of discrete-time systems with iteration-varying trajectory and random initial condition," *Automatica*, vol. 44, no. 8, pp. 2207–2213, Aug. 2008.
[33] X.-D. Li, T. W. S. Chow, and L. L. Cheng, "Adaptive iterative learning control of non-linear MIMO continuous systems with iteration-varying initial error and reference trajectory," *Int. J. Syst. Sci.*, vol. 44, no. 4, pp. 786–794, 2013.
[34] Q. Yan, J. Cai, Y. Ma, and Y. Yu, "Robust learning control for robot manipulators with random initial errors and iteration-varying reference trajectories," *IEEE Access*, vol. 7, pp. 32628–32643, 2019.
[35] L. Wu, Y. Yu, Z. Lin, Q. Yan, and X. Liu, "Time-varying boundary layer based iterative learning control for nonlinearly parametric time-delay systems with arbitrary initial errors and iteration-varying reference trajectories," *IEEE Access*, vol. 9, pp. 90642–90655, 2021.
[36] K. P. Tee, B. Ren, and S. S. Ge, "Control of nonlinear systems with time-varying output constraints," *Automatica*, vol. 47, no. 11, pp. 2511–2516, Nov. 2011.
[37] L. Liu, Y. J. Liu, S. C. Tong, and C. L. P. Chen, "Integral barrier Lyapunov function-based adaptive control for switched nonlinear systems," *Sci. China Inf. Sci.*, vol. 63, no. 3, pp. 1–14, Mar. 2020.
[38] J.-X. Xu and X. Jin, "State-constrained iterative learning control for a class of MIMO systems," *IEEE Trans. Autom. Control*, vol. 58, no. 5, pp. 1322–1327, May 2013.
[39] X. Jin and J.-X. Xu, "Iterative learning control for output-constrained systems with both parametric and nonparametric uncertainties," *Automatica*, vol. 49, no. 8, pp. 2508–2516, Aug. 2013.
[40] Q. Z. Yan and M. X. Sun, "Error-tracking iterative learning control with state constrained for nonparametric uncertain systems," *Control Theory Appl.*, vol. 32, no. 7, pp. 895–901, Jul. 2015.
[41] Q. Yu, Z. Hou, and R. Chi, "Adaptive iterative learning control for nonlinear uncertain systems with both state and input constraints," *J. Franklin Inst.*, vol. 353, no. 15, pp. 3920–3943, Oct. 2016.
[42] R. Chi, X. Liu, R. Zhang, Z. Hou, and B. Huang, "Constrained data-driven optimal iterative learning control," *J. Process Control*, vol. 55, pp. 10–29, Jul. 2017.
[43] X. Jin, "Iterative learning control for non-repetitive trajectory tracking of robot manipulators with joint position constraints and actuator faults," *Int. J. Adapt. Control Signal Process.*, vol. 31, no. 6, pp. 859–875, Jun. 2017.
[44] J. Liu, X. Dong, D. Huang, and M. Yu, "Composite energy function-based spatial iterative learning control in motion systems," *IEEE Trans. Control Syst. Technol.*, vol. 26, no. 5, pp. 1834–1841, Sep. 2018.
[45] Z. Li, C. Yin, H. Ji, and Z. Hou, "Constrained spatial adaptive iterative learning control for trajectory tracking of high speed train," *IEEE Trans. Intell. Transp. Syst.*, early access, Aug. 30, 2021, doi: 10.1109/TITS.2021.3106653.

YOUFANG YU received the B.S. degree in electronic engineering and the M.S. degree in agricultural electrification and automation from Zhejiang University, Hangzhou, in 1999 and 2006, respectively. From 1999 to 2003, she was a Lecturer with the Anhui Vocational and Technical College, Hefei. From 2006 to 2008, she was an Electronic Engineer with the Research and Development Department, Zhejiang Jincheng Technology Development Company Ltd., Hangzhou. Since 2008, she has been working with the Applied Engineering College, Zhejiang Business College, Hangzhou, where she is currently an Associate Professor. Her current research interests include automatic control, industrial automation, electronic technology, and biomass technology.

SONGHONG LAI received the B.S. degree in mechanical and electrical engineering from China Jiliang University, Hangzhou, in 2006, and the M.S. degree in mechanical and electrical engineering from the Zhejiang University of Technology, Hangzhou, in 2009. Since 2009, he has been working with the Applied Engineering College, Zhejiang Business College, Hangzhou, where he is currently a Lecturer. His current research interests include automatic control, industrial automation, and electronic technology.